Preclinical Evaluation of ^{11}C-Sarcosine as a Substrate of Proton-Coupled Amino Acid Transporters and First Human Application in Prostate Cancer

Morand Piert[1], Xia Shao[1], David Raffel[1], Mathew S. Davenport[1], Jeffrey Montgomery[2], Lakshmi Priya Kunju[3], Brian G. Hockley[1], Javed Siddiqui[3,4], Peter J.H. Scott[1], Arul M. Chinnaiyan[3,4], and Thekkelnaycke Rajendiran[3,4]

[1]Department of Radiology, University of Michigan, Ann Arbor, Michigan; [2]Department of Urology, University of Michigan, Ann Arbor, Michigan; [3]Pathology Department, University of Michigan, Ann Arbor, Michigan; and [4]Michigan Center for Translational Pathology, University of Michigan, Ann Arbor, Michigan

Sarcosine is a known substrate of proton-coupled amino acid transporters (PATs), which are overexpressed in selected tissues and solid tumors. Sarcosine, an *N*-methyl derivative of the amino acid glycine and a metabolic product of choline, plays an important role for prostate cancer aggressiveness and progression. **Methods:** ^{11}C-radiolabeled sarcosine was tested as a new PET imaging probe in comparison with ^{11}C-choline in 2 prostate cancer tumor xenograft models (DU-145 and PC-3). We characterized ^{11}C-sarcosine transport in PC-3 and LNCaP tumor cells and performed ^{11}C-sarcosine PET with CT in the first human subject with localized Gleason 4 + 3 prostate cancer. Target metabolite analyses of sarcosine and its natural precursors, glycine and choline, were performed from independent human prostate tissues. **Results:** In vitro assays indicated blockage of ^{11}C-sarcosine uptake into PC-3 and LNCaP tumor cells by excess unlabeled (cold) sarcosine. 5-hydroxy-L-tryptophan, but not 2-aminobicyclo-(2,2,1)-heptane-2-carboxylic acid, competitively inhibited ^{11}C-sarcosine tumor cell uptake, confirming PAT-mediated transport. In vivo tumor-to-background ratios (TBRs) obtained from ^{11}C-sarcosine PET were significantly elevated compared with ^{11}C-choline in DU-145 (TBR: 1.92 ± 0.11 for ^{11}C-sarcosine vs. 1.41 ± 0.13 for ^{11}C-choline [$n = 10$; $P < 0.002$]) and PC-3 tumors (TBR: 1.89 ± 0.2 for ^{11}C-sarcosine vs. 1.34 ± 0.16 for ^{11}C-choline [$n = 7$; $P < 0.002$]). ^{11}C-sarcosine produced high-contrast images in 1 case of localized clinically significant prostate cancer. Target metabolite analyses revealed significant stepwise increases of sarcosine, glycine, and choline tissue levels from benign prostate tissue to localized prostate cancer and subsequently metastatic disease. ^{11}C-sarcosine showed a favorable radiation dosimetry with an effective dose estimate of 0.0045 mSv/MBq, resulting in 2.68 mSv for a human subject (600-MBq dose). **Conclusion:** ^{11}C-sarcosine is a novel radiotracer for PATs and shows initial utility for prostate cancer imaging, with potential benefit over commonly used ^{11}C-choline.

Key Words: ^{11}C-sarcosine; prostate cancer; proton-coupled amino acid transporter (PAT)

J Nucl Med 2017; 58:1216–1223
DOI: 10.2967/jnumed.116.173179

The prostate cancer metabolome is characterized by an increased amino acid metabolism and a perturbation of nitrogen breakdown pathways (*1*), along with high total choline–containing compounds and phosphocholine levels (*2*). With metabolomic profiling, tissue levels of sarcosine—an *N*-methyl derivative of the amino acid glycine and a metabolic product of choline (Fig. 1)—have been found to be elevated in localized prostate cancer compared with benign prostatic tissues. Tissue sarcosine levels have also been shown to increase during prostate cancer progression to metastatic disease (*3*), and knockdown of glycine-*N*-methyltransferase—the enzyme that generates sarcosine from glycine—attenuates prostate cancer invasion. The addition of exogenous sarcosine, or knockdown of the mitochondrial enzyme that leads to sarcosine degradation (sarcosine dehydrogenase [SARDH]), induces an invasive phenotype in benign prostate epithelial cells (*4*). Furthermore, there is evidence for a strong sarcosine-related induction of genes involved particularly in cell cycle progression (*5*). Sarcosine is therefore thought to be a potential oncometabolite rather than a nonproteinogenic amino acid (*6*).

These data suggest a potential role of radiolabeled sarcosine for PET imaging. ^{11}C-choline and ^{18}F-fluorocholine are widely used PET radiopharmaceuticals for imaging of prostate cancer, particularly in the setting of prostate cancer recurrence (*7*). At primary staging, ^{11}C-choline preferentially identifies intermediate- and high-risk (i.e., clinically significant) prostate cancer, whereas low-risk lesions are typically not visualized (*8,9*). However, choline radiotracers are limited because of commonly observed increased retention in nodular benign prostatic hyperplasia (*10*) as well as unsatisfactory accuracy for nodal metastatic disease in initial staging (*11*).

The purpose of this study was to assess the uptake mechanism of ^{11}C-sarcosine, to test its utility in common prostate cancer xenograft models in comparison to ^{11}C-choline using small-animal PET, and to provide first human evidence of its potential in localized prostate cancer.

MATERIALS AND METHODS

Radiotracer Synthesis

^{11}C-choline was synthesized by ^{11}C-methylation of *N,N*-dimethylaminoethanol with ^{11}C-methyl iodide (*12*), whereas ^{11}C-acetate was prepared by bubbling ^{11}C-CO_2 through a solution of methyl-magnesium chloride (*13*).

Received Dec. 7, 2016; revision accepted Feb. 14, 2017.
For correspondence contact: Morand Piert, University of Michigan Health System, Department of Radiology, Division of Nuclear Medicine, University Hospital B1G505C, 1500 E. Medical Center Dr., Ann Arbor, MI 48109-0028.
E-mail: mpiert@umich.edu
Published online Mar. 16, 2017.

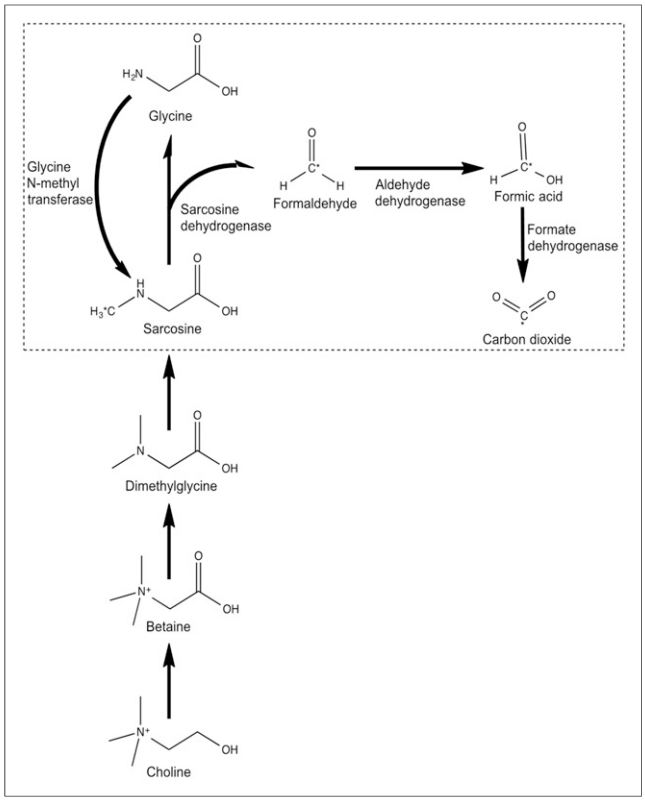

FIGURE 1. Sarcosine metabolism. C* = radiolabel.

We radiolabeled ^{11}C-sarcosine by our standard ^{11}C-methylation method using ^{11}C-methyl triflate (*14*), followed by saponification using aqueous sodium hydroxide at 60°C (Fig. 2). After labeling, the reaction mixture was diluted with water and purified using an anion-exchange solid-phase extraction cartridge. The final injectable dose was eluted with aqueous sodium chloride and filtered through a 0.22-μm sterile filter. Total synthesis time was approximately 25 min. Non–decay-corrected radiochemical yield was 2.5%–6% (non–decay-corrected yield based on 111 GBq of ^{11}C-CO_2, $n = 5$), and radiochemical purity was greater than 95%. Radiochemical identity was confirmed and quantified by standard high-performance liquid chromatography (i.e., calculating relative retention times). The mass of ^{11}C-sarcosine for human use was 10 nmol or less.

Cell Culture and Animal Experiments

All animal experiments were conducted in accordance with the Institutional Commission on the Ethical Treatment of Animals. Androgen receptor–positive (LNCaP) and –negative (DU-145 and PC-3) prostate cancer cell lines were obtained from American Type Culture Collection, and chemicals were purchased from Sigma-Aldrich. Genetically fingerprinted androgen receptor–positive (LNCaP) and –negative (DU-145, PC-3) prostate cancer cell lines were cultured in RPMI-1640 medium in the presence of 10% heat-inactivated fetal bovine serum, 1% penicillin/streptomycin, 2 mMol L-glutamine, and 1 mMol sodium pyruvate. Approximately 5 million LNCaP, DU-145, or PC-3 cells were injected into the flanks of 6- to 8-wk-old athymic *nu/nu* mice (Charles River). Animals were housed under pathogen-free conditions in microisolator cages, with rodent chow and water available ad libitum. Animals were examined daily, and body weight and tumor size were determined. The tumors were allowed to grow to a diameter of 4–6 mm (short axis) before imaging.

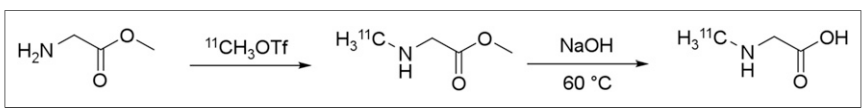

FIGURE 2. Synthesis of *N*-^{11}C-methylglycine.

^{11}C-Sarcosine Cell Assays

The ^{11}C-sarcosine uptake of approximately 3×10^5 PC-3 and LNCaP tumor cells was determined (in triplicates) with and without the presence of increasing concentrations of unlabeled sarcosine. To determine the precision of uptake measurements, PC-3 cells were incubated in RPMI-1640 medium for 20 min with 9 kBq of ^{11}C-sarcosine, washed 3 times with ice-cold phosphate-buffered saline, and counted. The ^{11}C-sarcosine uptake was determined to be 12.5% ± 1.1% of the administered dose ($n = 12$). ^{11}C-sarcosine uptake was then determined using specific competitive inhibitors of 2 amino acid transporter systems, 5-hydroxy-L-tryptophan (HT) for the proton-coupled amino acid transporters (PAT1 gene symbol SLC36A1, PAT2 gene symbol SLC36A2, PAT4 gene symbol SLC36A4) (*15*) and 2-aminobicyclo-(2,2,1)-heptane-2-carboxylic acid (BCH) for system L (*16*). Thereafter, ^{11}C-sarcosine was added to cells for 20 min and washed 3 times before counting. Using trypan blue staining, we found cell vitality intact (>95%) after incubation and washing for all samples.

^{11}C-Sarcosine Biodistribution

The biodistribution and organ kinetics of ^{11}C-sarcosine were measured in normal rats and used to estimate human radiation-absorbed doses according to previously described methods (*17*). Briefly, the organ distribution of ^{11}C-sarcosine was determined in 2 male and 2 female Sprague–Dawley rats at 5 time points (5, 15, 30, 60, and 90 min) using injected doses of 7.4–28 MBq of ^{11}C-sarcosine. Groups of animals were sacrificed while under isoflurane anesthesia. Organs were quickly removed, weighed, and sectioned for γ-counting. The kinetics of elimination of ^{11}C-sarcosine through urinary excretion were measured with dynamic PET imaging of the bladder in 4 rats (microPET P4 scanner; Siemens). A 1-phase exponential association model was fitted to urinary bladder time–activity data to determine the fraction of the injected dose excreted into urine. The OLINDA/EXM 1.0 software package was used to generate human radiation absorbed dose estimates from the rat biodistribution kinetic data and the urinary excretion data, applying a 4.0-h bladder-voiding interval (*18*).

Radiolabeled Sarcosine Metabolites

High-performance liquid chromatography was performed to assess for radiolabeled ^{11}C-sarcosine metabolites in blood and tissue homogenates of rat prostate and pancreas. On the basis of the known tissue metabolism of sarcosine as a methyl donor, a certain fraction of ^{11}C-sarcosine is expected to be metabolized to ^{11}C-CO_2 and exhaled (*19*). We measured the cumulative exhaled radioactivity for ^{11}C-sarcosine ($n = 2$), in comparison to ^{11}C-acetate ($n = 1$) and ^{11}C-choline ($n = 1$) as negative control. The radioactivity in breathing air was captured with a commercial activated charcoal filter (EnviroPure) using a closed system and placed into the microPET scanner for 60 min to measure cumulative time–activity curves of exhaled air.

We also analyzed volatile radioactivity in tissues, assuming them to be ^{11}C-CO_2. Blood, pancreas, and prostate were collected and split into 2 preweighted vials. One was sealed immediately, whereas the other was treated with

$HClO_4$ (0.8 N) and homogenized. Nitrogen gas was then passed through the mixture for 2 min at about a 10 mL/min flow rate to evaporate the volatile metabolite. The percentage of volatile metabolite from each sample was calculated on the basis of activity loss and tissue weight.

Target Metabolite Analyses

Absolute quantification of choline, glycine, and sarcosine in tumor tissue was determined by target metabolite validation using assays based on gas chromatography–mass spectrometry in human prostate cancer tissues and compared with normal prostate tissues collected by the institutional prostate tissue core. Briefly, frozen tissues were homogenized in methanol after being spiked with labeled internal standards (d^3-sarcosine and ^{13}C-glycine) and extracted using a 1:1 volume ratio of water to chloroform. The aqueous methanolic layer was collected and dried, and the extract was azeotroped twice with dimethylformamide. Dimethylformamide (100 μL) and *N*-methyl-*N*-*tert*-butylmethylsilyltrifluoroacetamide + 1% t-butyl-dimethylchlorosilane were added and incubated at 60°C for 1 h. Selective ion monitoring was used for quantification. The amount of sarcosine and glycine was quantified by measuring the peak area of the native sarcosine (m/z = 232) to that corresponding to spiked isotope-labeled sarcosine (m/z = 235) and the native glycine (m/z = 218) to that of spiked labeled glycine (m/z = 219), respectively. The levels of sarcosine and glycine were normalized to the tissue weight (in nmol/mg).

Choline was extracted from tissues by liquid–liquid extraction ($MeOH:H_2O:CHCl_3$, 1:1:1 ratio). Tissues were homogenized after the internal standard (^{13}C, d^4- choline chloride) was spiked. The aqueous methanolic layer containing choline was evaporated to dryness. After being cooled, 50 μL of pyridine and 100 μL of *N,O*-Bis(trimethylsilyl)trifluoroacetamide were added and heated at 70°C for 60 min. The reaction mixture was dissolved in ethyl-acetate and injected for gas chromatography–mass spectrometry. The amount of choline was calculated by measuring the peak area of the native choline (m/z = 146) to that corresponding to spiked isotope-labeled choline (m/z = 151).

^{11}C-Sarcosine and ^{11}C-Choline Small-Animal PET

Nude mice bearing DU-145 (n = 10) and PC-3 (n = 7) tumors received ^{11}C-sarcosine (27.2 ± 13 kBq) intravenously through a bolus tail injection, and 30-min dynamic small-animal PET was performed. After near-complete decay to less than 2% of the initial dose, a dynamic ^{11}C-choline (28 ± 9 kBq) scan was obtained in the same position to ascertain identical tumor position between scans and to avoid bias due to rapidly growing tumors.

Data Reconstruction and Analysis

Images were corrected for decay, scatter, and photon attenuation using a ^{68}Ge rod source. Time–activity curves of volumes of interest were obtained from dynamic image datasets defined for major organs and tumors to calculate tumor–to–muscle background ratios (TBR). The inspection of time–activity data indicated that the TBRs of ^{11}C-sarcosine and ^{11}C-choline were relatively stable between 5 and 20 min. We therefore selected this time interval for the comparison of the TBRs of both tracers.

First Human Subject

After internal review board approval and obtaining written consent, a patient with Gleason 4 + 3 primary prostate cancer received 606 MBq of ^{11}C-sarcosine for PET/CT scanning (Biograph 40 TrueV mCT; Siemens). Anatomic 3-T MRI was performed separately (Ingenia; Philips). PET data were registered with the 3-dimensional T2-weighted MRI using commercial software (MIM Maestro Software) (*20,21*). The 3-dimensional T2-weighted sequence was then used for targeted transrectal prostate biopsies with a commercial system (UroNav; Invivo).

Statistics

Statistical analyses were performed using JMP 12 (SAS). For paired data (^{11}C-sarcosine vs. ^{11}C-choline), a paired Wilcoxon test was performed. For tissue metabolites, ANOVA followed by Student–Newman–Keuls tests were performed. Data are presented as mean ± SD, when appropriate, and P values less than 0.05 were considered statistically significant.

TABLE 1
Biodistribution of ^{11}C-Sarcosine in Major Organs of Rats (%ID/g)

Organ	5 min	15 min	30 min	60 min	90 min
Brain	0.090 ± 0.021	0.109 ± 0.014	0.138 ± 0.042	0.114 ± 0.031	0.115 ± 0.051
Eyeballs	0.194 ± 0.034	0.212 ± 0.028	0.168138 ± 0.049	0.115 ± 0.030	0.111 ± 0.022
Heart	0.462 ± 0.130	0.455 ± 0.028	0.325138 ± 0.040	0.217 ± 0.036	0.198 ± 0.049
Lung	1.049 ± 0.126	1.159 ± 0.179	0.821138 ± 0.145	0.531 ± 0.056	0.467 ± 0.094
Liver	1.291 ± 0.541	1.100 ± 0.354	1.013138 ± 0.417	0.633 ± 0.169	0.662 ± 0.159
Pancreas	1.068 ± 0.618	1.218 ± 0.370	1.106 ± 0.153	1.045 ± 0.695	0.960 ± 0.551
Spleen	0.626 ± 0.041	0.623 ± 0.125	0.493 ± 0.041	0.392 ± 0.011	0.398 ± 0.091
Adrenal	0.620 ± 0.166	0.555 ± 0.021	0.503 ± 0.056	0.398 ± 0.153	0.474 ± 0.318
Kidney	3.004 ± 1.114	2.776 ± 0.607	1.774 ± 0.362	1.260 ± 0.254	0.956 ± 0.129
Stomach	1.032 ± 0.319	1.033 ± 0.074	0.861 ± 0.169	0.610 ± 0.097	0.541 ± 0.050
Ovary*	0.863 ± 0.170	0.786 ± 0.031	0.727 ± 0.063	0.432 ± 0.004	0.375 ± 0.008
Uterus*	0.724 ± 0.068	0.508 ± 0.200	0.447 ± 0.169	0.522 ± 0.220	0.181 ± 0.018
Testes*	0.071 ± 0.054	0.172 ± 0.012	0.122 ± 0.007	0.114 ± 0.025	0.079 ± 0.001
Muscle	0.140 ± 0.040	0.206 ± 0.015	0.224 ± 0.047	0.226 ± 0.067	0.164 ± 0.032
Bone	0.752 ± 0.543	0.604 ± 0.071	0.506 ± 0.076	0.37 ± 0.038	0.265 ± 0.101
Blood	0.396 ± 0.247	0.423 ± 0.028	0.245 ± 0.054	0.179 ± 0.034	0.196 ± 0.035

*n = 2 animals used for these values.

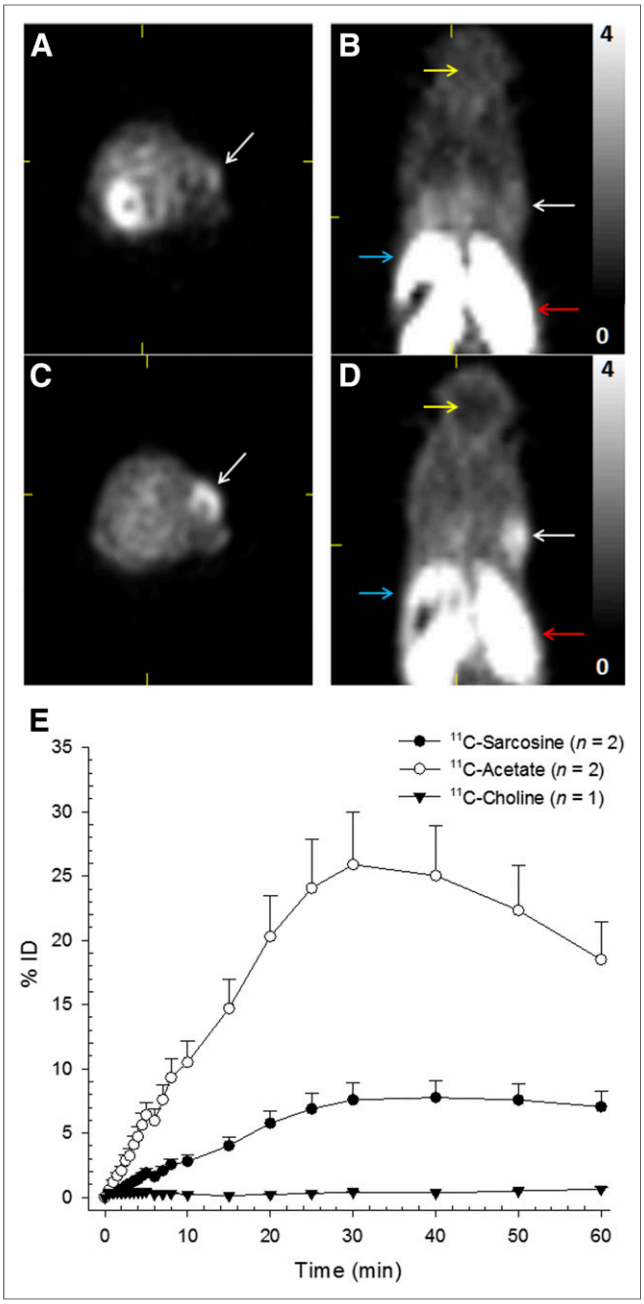

FIGURE 3. ^{11}C-sarcosine and ^{11}C-choline small-animal PET. Improved visualization of a DU-145 tumor (white arrows) and lower hepatic uptake (blue arrows) after intravenous injection of 16.3 MBq of ^{11}C-sarcosine (C and D) compared with 16.8 MBq of ^{11}C-choline (A and C) on transaxial (A and C) and coronal (B and D) small-animal PET images (summed data 5–20 min; SUV range, 0–4). Both tracers display intense renal uptake (red arrows). Brain uptake (yellow arrows) is essentially absent for ^{11}C-sarcosine, whereas ^{11}C-choline brain uptake is low. Cumulative exhaled mean (±SD) radioactivity (as % injected dose) representing ^{11}C-CO_2 (E) was measured in healthy rats after intravenous injection of ^{11}C-sarcosine (•), ^{11}C-acetate (○), and ^{11}C-choline (▾).

RESULTS

Small-Animal PET

Both ^{11}C-sarcosine and ^{11}C-choline showed intense radiotracer uptake in the intestine and kidneys (Table 1). Similar to ^{11}C-choline, the urinary excretion of radioactivity from ^{11}C-sarcosine was limited. ^{11}C-sarcosine liver uptake was elevated compared with the mediastinum, but was markedly lower than the hepatic ^{11}C-choline uptake. Low ^{11}C-choline uptake was noted in the brain, but ^{11}C-sarcosine uptake in the brain was nearly absent (Fig. 3).

Time–activity curves of ^{11}C-sarcosine showed rapid tumor uptake in both tumor models, with relatively stable TBR at 5 min after injection. All 17 DU-145 and PC-3 tumors were visually identified on ^{11}C-sarcosine PET, but only 12 of 17 (71%) were noted with ^{11}C-choline. The TBR (at 5–20 min) for ^{11}C-sarcosine was significantly elevated compared with ^{11}C-choline in both tumors models (Fig. 3). The ^{11}C-sarcosine TBR of DU-145 tumors was 1.92 ± 0.11 compared with 1.41 ± 0.13 for ^{11}C-choline ($P < 0.002$). Similarly, the TBR of PC-3 tumors was 1.89 ± 0.2 for ^{11}C-sarcosine and 1.34 ± 0.16 for ^{11}C-choline ($P < 0.002$).

Cell Assays

The ^{11}C-sarcosine uptake of PC-3 and LNCaP cells could be blocked with an excess of nonradiolabeled (cold) sarcosine (LNCaP: decrease to 3.2% ± 0.7% at 1.125 mMol/mL; PC-3: decrease to 1.1% ± 0.4% at 7.5 mMol/mL), confirming a specific

TABLE 2
Radiation-Absorbed Dose Estimates for ^{11}C-Sarcosine

Target organ	Total dose	
	mGy/MBq	rad/mCi
Adrenals	0.0040	0.015
Brain	0.0021	0.008
Breasts	0.0021	0.008
Gallbladder wall	0.0038	0.014
Lower large intestine wall	0.0034	0.013
Small intestine	0.0145	0.054
Stomach wall	0.0041	0.015
Upper large intestine wall	0.0066	0.025
Heart wall	0.0031	0.012
Kidneys	0.0115	0.042
Liver	0.0066	0.024
Lungs	0.0050	0.018
Muscle	0.0025	0.009
Ovaries	0.0065	0.024
Pancreas	0.0066	0.024
Red marrow	0.0024	0.009
Osteogenic cells	0.0035	0.013
Skin	0.0020	0.007
Spleen	0.0040	0.015
Testes	0.0023	0.009
Thymus	0.0025	0.009
Thyroid	0.0024	0.009
Urinary bladder wall	0.0086	0.032
Uterus	0.0057	0.021
Total body	0.0028	0.011
Effective dose	0.0045 (mSv/MBq)	0.017 (rem/mCi)

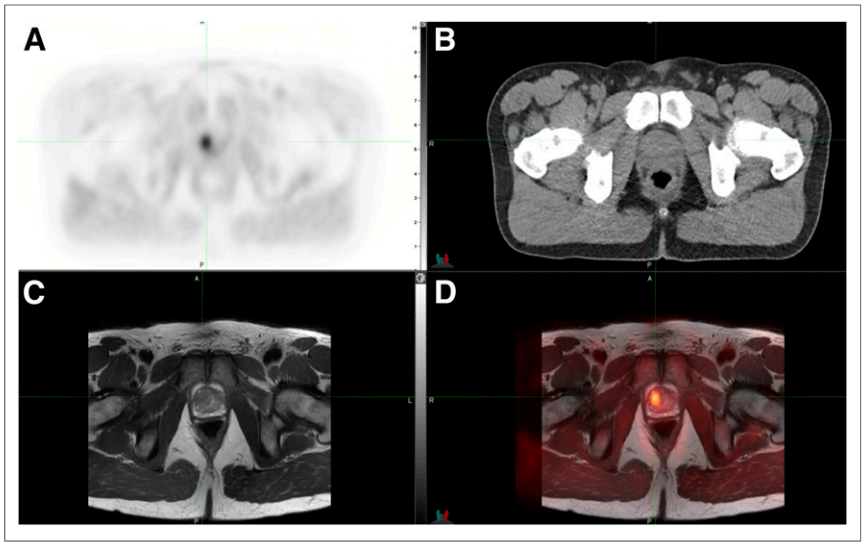

FIGURE 4. Human ^{11}C-sarcosine PET. Transaxial ^{11}C-sarcosine hybrid PET/CT showed a (triangulated) adenocarcinoma in the transition zone of anterior right prostate gland on PET (A), CT (B), and separately obtained T2-weighted MR sequence (C) with resulting PET/MRI registration (D).

transport mechanism of sarcosine into cells. The PAT inhibitor HT and the system L inhibitor BCH were tested at 0.015 mMol/mL concentrations. After HT incubation, ^{11}C-sarcosine uptake of PC-3 cells decreased to 22.7% ± 7.6% in a dose-dependent fashion. ^{11}C-sarcosine uptake of LNCaP cells could be almost completely blocked by HT to 9.6% ± 4.3% compared with controls, confirming PAT-dependent transport of ^{11}C-sarcosine. Because sarcosine is not an L-amino acid, BCH had little effect on ^{11}C-sarcosine uptake of both cell lines (reduction to 87.9% ± 33.6% for PC-3 and to 85.0% ± 13.0% for LNCaP).

Radiation Dosimetry Estimates

The biodistribution of ^{11}C-sarcosine obtained from rats was used to calculate human radiation absorbed dose estimates (Table 1). The maximum percentage injected dose observed in the gastrointestinal tract (9.0%) was assumed to enter the small intestine. Also, on the basis of separate rat small-animal PET studies, 2.6% ± 1.4% of the injected dose were excreted via the urinary bladder with a biologic half-time of 0.152 ± 0.081 h. Absorbed dose estimates are shown for the reference adult male organ model in Table 2. The organs with the highest absorbed dose estimates were the small intestine followed by the kidneys. The effective dose was 0.0045 mSv/MBq, resulting in 2.68 mSv for human subjects (at 600 MBq administered dose).

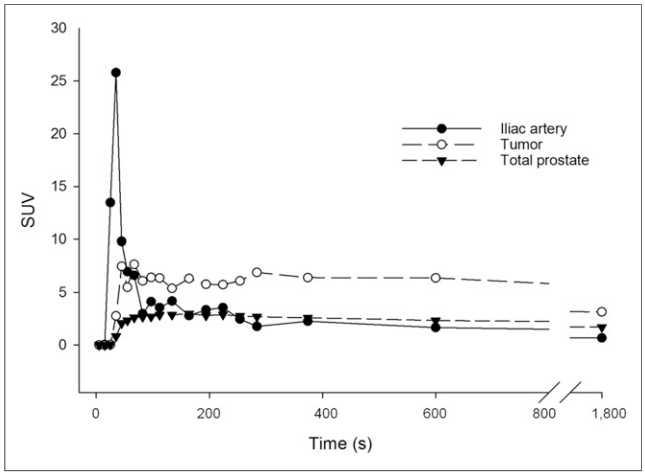

FIGURE 5. Human ^{11}C-sarcosine time–activity curves. Time–activity curves of human subject indicated rapid tumor uptake of ^{11}C-sarcosine (○) after delivery via iliac artery (●).

Radiolabeled Metabolite Analyses

No aqueous radiolabeled metabolites of ^{11}C-sarcosine in blood, prostate, or pancreas were detected at any time point. We concluded that the radiolabeled methyl-group of ^{11}C-sarcosine is eliminated from the aqueous pool because of SARDH-mediated conversion to glycine (Fig. 1). This was further substantiated by capturing radioactivity in the exhaled air, indicating production of ^{11}C-CO_2. Cumulative time–activity curves obtained from expiratory air indicated that approximately 7% of the injected dose was exhaled as ^{11}C-CO_2 over a period of 60 min, which was markedly less compared with ^{11}C-acetate, another known methyl-donor. In the case of ^{11}C-acetate, the filter was unable to capture all exhaled ^{11}C-CO_2 from ^{11}C-acetate (Fig. 3E). The cumulative time–activity curve obtained after ^{11}C-sarcosine administration was flat from about 30 to 60 min, indicating that practically all ^{11}C-CO_2 was exhaled within 30 min. The amount of radioactivity detected in the expired air after ^{11}C-choline administration (as negative control) was negligible.

We further determined the volatile ^{11}C-CO_2 fraction of radioactivity within blood, pancreas, and prostate in 1 animal per time point (15, 30, and 60 min after administration). The ^{11}C-CO_2 fraction ranged from 14% to 21% in blood, 9% to 23% in prostate, and 12% to 24% in pancreas. Thus, a substantial majority of radioactivity was related to ^{11}C-sarcosine and not ^{11}C-CO_2 in every measured tissue at all time points.

Human Subject

Figure 4 shows hybrid PET/CT images of the first human subject injected with ^{11}C-sarcosine. Early-time-point images (between 5 and 10 min after injection) displayed focally increased uptake in the right anterior transition zone of the prostate gland and no significant uptake within contralateral benign prostatic hyperplasia nodules. Registration of PET with T2-weighted MR images revealed a low-signal intensity lesion at this location, measuring 1.04 mL on T2-weighted MR. A Gleason 4 + 3 prostate cancer was identified using image-guided prostate biopsy, whereas standard biopsies were negative. Time–activity curves demonstrated preferential ^{11}C-sarcosine uptake in the tumor compared with the total prostate and the arterial blood with stable lesion-to-background ratio over time (Fig. 5).

Metabolite Analyses

Human prostate tissue concentrations of choline (n = 6) increased significantly from benign (0.17 ± 0.05) to localized (0.28 ± 0.08) and metastatic (0.42 ± 0.08 nmol/mg) prostate cancer (statistical significance levels as listed in Fig. 6). Similarly, glycine

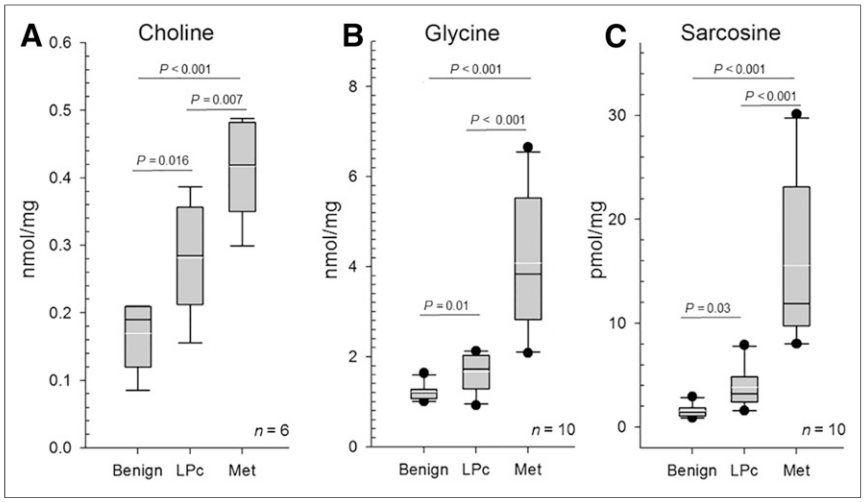

FIGURE 6. Target metabolite analyses. Whisker plots (white lines: mean [±95% confidence interval]; black line: median; black dots: outliers) of tissue concentrations for choline (A), glycine (B), and sarcosine (C) obtained from human localized (LPc) and metastatic (Met) prostate cancer in comparison to benign prostate tissues (Benign).

(n = 10) showed significant stepwise increases from benign prostate tissues (1.21 ± 0.18) to localized (1.67 ± 0.41) to metastatic (4.07 ± 1.53 nmol/mg) prostate cancer, with sarcosine (n = 10) displaying the largest gains (benign: 1.54 ± 0.6; localized: 3.82 ± 2.08; metastatic prostate cancer: 15.57 ± 8.0 pmol/mg).

DISCUSSION

We identified increased ^{11}C-sarcosine uptake (relative to background) in 2 preclinical human prostate cancer xenograft models, with moderate improvement over ^{11}C-choline. Furthermore, initial human data are promising in a case of low-volume organ-confined prostate cancer, further substantiating a utility for human use. We considered ^{11}C-sarcosine for prostate cancer imaging because metabolomic data indicated strongly elevated tissue levels in localized prostate cancer, particularly in metastatic disease (*3*). Also, the mere addition of sarcosine to cultured benign prostate epithelial cells induced an invasive phenotype (*4*). Although the sarcosine metabolism is well-characterized, its metabolic functions in the human body are still poorly understood and are currently under active investigation (*5,22*).

Radiolabeled ^{11}C-sarcosine is chemically identical to the nonproteinogenic amino acid sarcosine. The known metabolism of (unlabeled) sarcosine consists of 2 biochemical pathways occurring in mitochondria. The first pathway is the oxidative pathway of choline via betaine and dimethylglycine (Fig. 1). Here, the enzyme SARDH plays a critical role in the conversion to glycine. The second pathway involves methionine with donation of a methyl-group via *S*-adenosylmethionine to glycine. Here, glycine *N*-methyltransferase acts as an essential component that influences synthesis of sarcosine from glycine (*23*). Because ^{11}C-sarcosine is not a substrate in either pathway, we consider ^{11}C-sarcosine cell uptake not to reflect the activity of these sarcosine production pathways.

Sarcosine is a known ligand of the PAT family, which are thought to be multipurpose carriers with distinct roles in different cells (*24*). PAT1/PAT2 are low-affinity carriers that mediate 1:1 symport of protons and small amino acids such as glycine, alanine, proline (*25*), and γ-aminobutyric acid into neurons. PAT4 is a high-affinity, low-capacity electroneutral transporter of neutral amino acids (*26*). Baseline PAT expression is ubiquitous (*15*) and resides at the cell surface and intracellular membranes (endosomes, lysosomes) (*27*). Elevated PAT expressions have been linked to cell proliferation (*24*). Here, PATs function as part of an amino acid–sensing engine that drives activation of the mammalian target of rapamycin complex 1 (mTORC1) (*27*). Physiologically high PAT1/PAT2 expressions have been identified in the brain, pancreas, kidney, duodenum, and small intestine (*24*). SLC36A2 expression has been documented at the apical surface of the human proximal renal tubule, where PAT2 functions in the reabsorption of amino acids (*24*). Within the intestinal tract, PAT1 plays an important role as nutrient and drug transporter (*28*). PAT4 (SLC36A4) is abundantly expressed in excitatory and inhibitory neurons as well as epithelial cells (*26*). In cancer, PAT4 is particularly important for the amino acid–dependent activation of the mTORC1 pathway, which is upregulated in prostate and colon cancer, where PAT4 overexpression has been linked to an aggressive phenotype (*29*).

In prostate cancer cells, ^{11}C-sarcosine uptake could be blocked with cold sarcosine, which confirmed a specific transport mechanism for sarcosine and suggests transport as the rate-limiting step. The dose-dependent inhibition of ^{11}C-sarcosine uptake by the PAT inhibitor HT and the lack of significant inhibition by BCH are consistent with the literature surrounding sarcosine. Although we have not verified PAT expression in the tested PC-3 and LNCaP cancer cell lines, we nevertheless concluded that transport of ^{11}C-sarcosine into cells is PAT-mediated.

The ^{11}C-sarcosine biodistribution in normal rats indicated elevated uptake in the pancreas and kidneys; moderate uptake in the liver, stomach, lungs, and adrenals; and low uptake in all other major parenchymal organs. The elevated ^{11}C-sarcosine uptake in the pancreas and kidneys is likely related to PAT1/PAT2-regulated transport. However, ^{11}C-sarcosine uptake in rat brain was found to be low despite neuronal PAT1 expression. Also, organs with elevated SARDH protein expression (high protein levels are found in the liver, pancreas and adrenal glands (*30*)) might also have elevated ^{11}C-sarcosine uptake, which—based on our biodistribution data—appears to be the case.

Radiation dosimetry estimates for ^{11}C-sarcosine resulted in an effective dose of 0.0045 mSv/MBq, which is similar to that of ^{11}C-choline and compares favorably to ^{18}F-FDG and many other ^{11}C-labeled radiopharmaceuticals (*31*). Our absorbed radiation dose measurements confirmed that ^{11}C-sarcosine can be safely administered to humans.

^{11}C-choline and ^{18}F-fluorocholine are widely used PET radiotracers for prostate cancer imaging (*9,20*), but also ^{11}C-methionine and ^{11}C-acetate PET have been successfully tested for this indication (*32,33*). ^{11}C-choline is known to be rapidly transported into human cancers, including prostate cancer. Although the uptake of ^{11}C-choline has been linked to the choline kinase activity in prostate cancer (*34*), a substantial fraction of ^{11}C-choline may remain nonmetabolized intracellularly (*35*), indicating that choline transport and not phosphorylation may be key to ^{11}C-choline uptake

into certain cancer cells. In this context, one potential basis for elevated sarcosine tissue levels would be the upregulation of the oxidative pathway of choline to glycine. In fact, when ^{11}C-choline was used, it was determined that oxidation of choline is the dominant metabolic pathway in HCT116 tumor xenografts (*36*). Our data obtained from human tissues indicate significantly increased choline, sarcosine, and glycine tissue levels in prostate cancer and particularly in metastatic disease compared with benign prostatic tissues. These data are compatible with an upregulation of both metabolic pathways leading to sarcosine production: the methylation from glycine via glycine-*N*-methyltransferase and the oxidative pathway of choline. Although activation of these pathways will increase the sarcosine tissue concentration, we consider the ^{11}C-sarcosine uptake only to reflect PAT transport activity and not the magnitude of the sarcosine tissue pool.

Our metabolite analyses did not reveal any radiolabeled aqueous metabolites in blood and tissue. We attribute this finding to the fact that with the demethylation of ^{11}C-sarcosine to glycine by SARDH, the radiolabeled carbon group is ultimately converted to ^{11}C-CO_2. Therefore, the measured tissue radioactivity will be determined largely by the sum of (unchanged) ^{11}C-sarcosine and ^{11}C-CO_2. Because ^{11}C-CO_2 will gradually be removed from tissues, it is unclear whether the decrease of radioactivity from tissue over time (as identified by biodistribution studies) is related to ^{11}C-sarcosine or ^{11}C-CO_2. However, we do not believe that the decline in the radioactivity noted in many organs is related to a significant loss of ^{11}C-CO_2 (Table 1). Such declines are commonly seen for many ^{11}C-labeled radiopharmaceuticals without ^{11}C-CO_2 production, including ^{11}C-choline as unbound radioactivity is escaping back into the vasculature. Because tissues were quickly excised and placed into air-tight vials for biodistribution, a potential for a loss of radioactivity due to ^{11}C-CO_2 evaporation was minimized. In fact, the lack of such decline from tumor tissue, in contrast to benign prostate tissues as seen in Figure 5, may not only indicate prostate cancer, but also may have adverse prognostic implications. First, elevated sarcosine tissue levels and enzymes related to the sarcosine metabolism have been linked to tumor aggressiveness not only in prostate cancer (*3,4*), but also in breast and hepatocellular carcinomas in which increased glycine *N*-methyltransferase protein expression has been associated with decreased survival (*37,38*). Thus, we postulate that ^{11}C-sarcosine kinetics (displaying a loss of radioactivity from tumor tissue over time), whether due to demethylation of ^{11}C-sarcosine by SARDH resulting in ^{11}C-CO_2 production or due to an equilibrium of ^{11}C-sarcosine with (low) intracellular nonlabeled sarcosine levels, might indicate less aggressive tumor features and may have prognostic value.

CONCLUSION

Despite significant progress, the understanding of PATs and their signaling functions is far from complete. The importance of the activity of SLC36 family amino acid (PAT) transporters in cell proliferation and cancer has only recently been fully recognized (*22*). Here, our data suggest that PAT-mediated sarcosine transport is key to ^{11}C-sarcosine uptake in prostate cancer. ^{11}C-sarcosine PET allows the assessment of PAT transport in the human body with apparent utility in cancer imaging. The improved tumor visualization with ^{11}C-sarcosine compared with ^{11}C-choline seen in xenograft tumor models together with increased sarcosine tumor tissue levels compared with benign prostate tissues indicate a potential role for ^{11}C-sarcosine PET in human prostate cancer. If proven successful with further human use, this radiotracer exemplifies a new concept for PET imaging of cancer based on proton-coupled SLC36 family amino acid transporters currently undergoing active research.

DISCLOSURE

This study was funded by NIH R21CA191052-01, NIH DK097153, and a seed grant of the Radiology Department of the University of Michigan. No other potential conflict of interest relevant to this article was reported.

ACKNOWLEDGMENTS

We thank the staff of the clinical and preclinical PET suites for their excellent technical support.

REFERENCES

1. Burton AJ, Tilling KM, Holly JM, et al. Metabolic imbalance and prostate cancer progression. *Int J Mol Epidemiol Genet.* 2010;1:248–271.
2. Swanson MG, Keshari KR, Tabatabai ZL, et al. Quantification of choline- and ethanolamine-containing metabolites in human prostate tissues using ^{1}H HR-MAS total correlation spectroscopy. *Magn Reson Med.* 2008;60:33–40.
3. Sreekumar A, Poisson LM, Rajendiran TM, et al. Metabolomic profiles delineate potential role for sarcosine in prostate cancer progression. *Nature.* 2009;457:910–914.
4. Khan AP, Rajendiran TM, Ateeq B, et al. The role of sarcosine metabolism in prostate cancer progression. *Neoplasia.* 2013;15:491–501.
5. Heger Z, Merlos Rodrigo MA, Michalek P, et al. Sarcosine up-regulates expression of genes involved in cell cycle progression of metastatic models of prostate cancer. *PLoS One.* 2016;11:e0165830.
6. Cha YJ. Kim do H, Jung WH, Koo JS. Expression of sarcosine metabolism-related proteins according to metastatic site in breast cancer. *Int J Clin Exp Pathol.* 2014;7:7824–7833.
7. Picchio M, Briganti A, Fanti S, et al. The role of choline positron emission tomography/computed tomography in the management of patients with prostate-specific antigen progression after radical treatment of prostate cancer. *Eur Urol.* 2011;59:51–60.
8. Park H, Wood D, Hussain H, et al. Introducing parametric fusion PET/MRI of primary prostate cancer. *J Nucl Med.* 2012;53:546–551.
9. Piert M, Park H, Khan A, et al. Detection of aggressive primary prostate cancer with ^{11}C-choline PET/CT using multimodality fusion techniques. *J Nucl Med.* 2009;50:1585–1593.
10. Souvatzoglou M, Weirich G, Schwarzenboeck S, et al. The sensitivity of [^{11}C] choline PET/CT to localize prostate cancer depends on the tumor configuration. *Clin Cancer Res.* 2011;17:3751–3759.
11. Piert M, El Naqa I, Davenport MS, Incerti E, Mapelli P, Picchio M. PET/MRI and prostate cancer. *Clin Transl Imaging.* 2016;4:473–485.
12. Shao X, Hockley B, Hoareau R, Schnau P, Scott PJH. High efficiency, fully automated preparation and quality control of [^{11}C]choline and [^{18}F]fluoromethylcholine for routine clinical application. *Appl Radiat Isot.* 2011;69:403–409.
13. Runkle AC, Shao X, Tluczek LJ, Henderson BD, Hockley BG, Scott PJ. Automated production of [^{11}C]acetate and [^{11}C]palmitate using a modified GE Tracerlab FX(C-Pro). *Appl Radiat Isot.* 2011;69:691–698.
14. Shao X, Kilbourn MR. A simple modification of GE Tracerlab FX C Pro for rapid sequential preparation of [^{11}C]carfentanil and [^{11}C]raclopride. *Appl Radiat Isot.* 2009;67:602–605.
15. Alexander SP, Benson HE, Faccenda E, et al. The concise guide to pharmacology 2013/14: transporters. *Br J Pharmacol.* 2013;170:1706–1796.
16. Kim CS, Cho SH, Chun HS, et al. BCH, an inhibitor of system L amino acid transporters, induces apoptosis in cancer cells. *Biol Pharm Bull.* 2008;31:1096–1100.
17. Jang KS, Jung YW, Gu G, et al. 4-[^{18}F]Fluoro-m-hydroxyphenethylguanidine: a radiopharmaceutical for quantifying regional cardiac sympathetic nerve density with positron emission tomography. *J Med Chem.* 2013;56:7312–7323.
18. Stabin MG, Sparks RB, Crowe E. OLINDA/EXM: the second-generation personal computer software for internal dose assessment in nuclear medicine. *J Nucl Med.* 2005;46:1023–1027.

19. Mitchell AD, Benevenga NJ. Importance of sarcosine formation in methionine methyl carbon oxidation in the rat. *J Nutr.* 1976;106:1702–1713.
20. Piert M, Montgomery J, Kunju LP, et al. ^{18}F-choline PET/MRI: the additional value of PET for MRI-guided transrectal prostate biopsies. *J Nucl Med.* 2016;57:1065–1070.
21. Meyer C, Ma B, Kunju LP, Davenport M, Piert M. Challenges in accurate registration of 3-D medical imaging and histopathology in primary prostate cancer. *Eur J Nucl Med Mol Imaging.* 2013;40(suppl 1):S72–S78.
22. Zheng L, Zhang W, Zhou Y, Li F, Wei H, Peng J. Recent advances in understanding amino acid sensing mechanisms that regulate mTORC1. *Int J Mol Sci.* 2016;17:1636–1651.
23. Cernei N, Heger Z, Gumulec J, et al. Sarcosine as a potential prostate cancer biomarker: a review. *Int J Mol Sci.* 2013;14:13893–13908.
24. Thwaites DT, Anderson CM. The SLC36 family of proton-coupled amino acid transporters and their potential role in drug transport. *Br J Pharmacol.* 2011;164:1802–1816.
25. Boll M, Daniel H, Gasnier B. The SLC36 family: proton-coupled transporters for the absorption of selected amino acids from extracellular and intracellular proteolysis. *Pflugers Arch.* 2004;447:776–779.
26. Roshanbin S, Hellsten SV, Tafreshiha A, Zhu Y, Raine A, Fredriksson R. PAT4 is abundantly expressed in excitatory and inhibitory neurons as well as epithelial cells. *Brain Res.* 2014;1557:12–25.
27. Ögmundsdóttir MH, Heublein S, Kazi S, et al. Proton-assisted amino acid transporter PAT1 complexes with Rag GTPases and activates TORC1 on late endosomal and lysosomal membranes. *PLoS One.* 2012;7:e36616.
28. Anderson CM, Grenade DS, Boll M, et al. H+/amino acid transporter 1 (PAT1) is the imino acid carrier: an intestinal nutrient/drug transporter in human and rat. *Gastroenterology.* 2004;127:1410–1422.
29. Stevens D, Verrill C, Bryant R, et al. The proton-assisted amino acid transporter 4 (PAT4/SLC36A4) is up-regulated in prostate cancer. *J Urol.* 2015;193:e677.
30. Bergeron F, Otto A, Blache P, et al. Molecular cloning and tissue distribution of rat sarcosine dehydrogenase. *Eur J Biochem.* 1998;257:556–561.
31. Tolvanen T, Yli-Kerttula T, Ujula T, et al. Biodistribution and radiation dosimetry of [^{11}C]choline: a comparison between rat and human data. *Eur J Nucl Med Mol Imaging.* 2010;37:874–883.
32. Tóth G, Lengyel Z, Balkay L, Salah MA, Tron L, Toth C. Detection of prostate cancer with ^{11}C-methionine positron emission tomography. *J Urol.* 2005;173:66–69.
33. Brogsitter C, Zophel K, Kotzerke J. ^{18}F-choline, ^{11}C-choline and ^{11}C-acetate PET/CT: comparative analysis for imaging prostate cancer patients. *Eur J Nucl Med Mol Imaging.* 2013;40(suppl 1):S18–S27.
34. Contractor K, Challapalli A, Barwick T, et al. Use of [^{11}C]choline PET-CT as a noninvasive method for detecting pelvic lymph node status from prostate cancer and relationship with choline kinase expression. *Clin Cancer Res.* 2011;17:7673–7683.
35. Bansal A, Shuyan W, Hara T, Harris RA, Degrado TR. Biodisposition and metabolism of [^{18}F]fluorocholine in 9L glioma cells and 9L glioma-bearing fisher rats. *Eur J Nucl Med Mol Imaging.* 2008;35:1192–1203.
36. Witney TH, Alam IS, Turton DR, et al. Evaluation of deuterated ^{18}F- and ^{11}C-labeled choline analogs for cancer detection by positron emission tomography. *Clin Cancer Res.* 2012;18:1063–1072.
37. Yoon JK, Kim do H, Koo JS. Implications of differences in expression of sarcosine metabolism-related proteins according to the molecular subtype of breast cancer. *J Transl Med.* 2014;12:149–160.
38. Lim SO, Park SJ, Kim W, et al. Proteome analysis of hepatocellular carcinoma. *Biochem Biophys Res Commun.* 2002;291:1031–1037.